Emergent Materials
https://doi.org/10.1007/s42247-025-01033-8

ORIGINAL ARTICLE

Comparing the osteogenic effects of sputtered titanium- and strontium titanate (STO)-modified polyetheretherketone

Masato Ikuta[1] · Anjar Anggraini Harumningtyas[2,3] · Tomoko Ito[2] · Kenta Fujita[2] · Takayuki Kitahara[1] · Masayuki Bun[1] · Takuya Furuichi[1] · Hiromasa Hirai[1] · Yuichiro Ukon[1] · Daisuke Tateiwa[4] · Yuya Kanie[1] · Masayuki Furuya[1] · Takahito Fujimori[1] · Seiji Okada[1] · Satoshi Hamaguchi[2] · Takashi Kaito[1]

Received: 5 November 2024 / Accepted: 6 February 2025

Abstract

Polyetheretherketone (PEEK) is widely used as an interbody cage due to its elastic modulus closely resembles that of human bone. However, its biological inertness is considered a major weakness, as it cannot directly bond with bone (lack of osseointegration capacity). Surface modification can impart bioactivity to PEEK while maintaining its mechanical properties. In this study, the surface of PEEK was modified with titanium or strontium titanate thin films formed by magnetron sputtering deposition. We evaluated the bone formation activity of strontium titanate-modified PEEK (PEEK-STO) by comparing three groups: unmodified PEEK (PEEK), titanium-modified PEEK (PEEK-Ti), and strontium titanate-modified PEEK (PEEK-STO). Osteogenic differentiation of cells, assessed by ALP activity, bone-related gene expression, and mineralization ability, demonstrated that PEEK-STO has the highest osteogenic activity. Furthermore, the evaluation of mineral deposition by non-cellular mechanisms using simulated body fluid showed that PEEK-Ti and PEEK-STO have higher calcium phosphate deposition capacity than PEEK. In vivo implantation of the materials into the rat femur demonstrated that bone-to-implant contact ratio (BIC%) and bone area ratio (BA%) in the proximity zone from the implant were significantly larger in PEEK-STO compared to PEEK-Ti and PEEK at 4 weeks post-surgery. This study demonstrates that surface modification of PEEK with strontium titanate through magnetron sputtering is an attractive option for solving the problems of PEEK's biological inertness while making the most of the advantages of PEEK as a spinal fusion device.

Keywords Polyetheretherketone · Strontium titanate · Surface modification · Magnetron sputtering · Osseointegration

1 Introduction

Age-related disc degeneration exacerbates spinal sagittal alignment due to decreased disc height [1]. Notably, as the impact of global spinal sagittal malalignment on patients' quality of life becomes more apparent, the number of cases of spinal intervertebral fusion, which restores disc height with intervertebral cages and fixes the spine with screws, is increasing [2, 3].

Material properties required for intervertebral cages include mechanical strength equivalent to human bone, initial fixation stability, and osseointegration-promoting properties [4, 5]. Currently, the primary materials used for interbody cages are polyetheretherketone (PEEK) and titanium or its alloys, each with advantages and disadvantages. PEEK played a central role in intervertebral cages until around 2010, largely due to its mechanical properties, including elastic modulus similar to human cancellous bone,

Masato Ikuta and Anjar Anggraini Harumningtyas contributed equally to this work.

✉ Satoshi Hamaguchi
hamaguch@ppl.eng.osaka-u.ac.jp

✉ Takashi Kaito
takashikaito@ort.med.osaka-u.ac.jp

[1] Department of Orthopedic Surgery, Osaka University Graduate School of Medicine, 2-2 Yamadaoka, Suita, Osaka 565-0871, Japan

[2] Division of Materials and Manufacturing Science, Graduate School of Engineering, Osaka University, 2-1 Yamadaoka, Suita, Osaka 565-0871, Japan

[3] Research Center for Advanced Materials, Research Organization for Nanotechnology and Material, National Research and Innovation Agency (BRIN), Jalan Babarsari Kotak Pos 6101 ykbb, Yogyakarta 55281, Indonesia

[4] Department of Orthopedic Surgery, Osaka International Medical & Science Center, 10-31 Kitayama-cho, Tennouji-ku, Osaka City, Osaka 543-0035, Japan

Published online: 25 February 2025

radiolucency, and chemical stability. However, its use has declined due largely to its biological inertness and inability to bond directly to bone [6–8]. Conversely, titanium is a corrosion-resistant metal with good biocompatibility and a higher bone-bonding rate than PEEK. Its disadvantages include a lack of radiolucency and a high elastic modulus, which can lead to subsidence into the vertebral bone, particularly in cases of compromised bone quality [9, 10].

Bone tissue bonds to the implant through osseointegration, which is the direct contact between bone and implant at the optical microscopic level, allowing forces on the implant to transfer directly to the bone [11, 12]. The presence of fibrous tissue between PEEK and bone can weaken this bond and reduce the mechanical strength [13, 14]. Against this background, various surface modifications have been made to overcome the weaknesses of PEEK, which has many excellent properties as a material [15]. As a representative example, surface modifications with hydroxyapatite and calcium phosphate, the main inorganic components of bone, enhance the biological activity of PEEK [14, 16]. Biomolecular modifications have been shown to enhance osteogenic activity. Modifying the quality of extracellular matrix proteins on PEEK promotes osteogenesis [17, 18]. Additionally, co-modification of the bone morphogenetic protein BMP-2 with phosphorylated gelatin has been shown to significantly enhance osteogenic activity [19]. Furthermore, the incorporation of angiogenic factors and adipocytokines facilitates osteogenic differentiation [20, 21]. In addition to biomolecular modifications, metal-based modifications have also been demonstrated to enhance osteogenic activity. Surface modifications using titanium and magnesium, as well as strontium (Sr), which will be discussed later, have been shown to promote bone formation [22–24]. Beyond chemical modifications, structural modifications such as surface nanostructuring and porosity enhancement have also been demonstrated to improve osseointegration [25, 26].

The thin film formation methods used for these surface modifications are categorized into three methods: physical vapor deposition (PVD), which involves directly vaporizing and depositing thin film materials; chemical vapor deposition (CVD), which utilizes chemical reactions with gas compounds containing thin film atoms; and wet coating methods using liquid phases [27, 28].

Magnetron sputtering, a type of PVD, has advantages that ensure consistent surface properties of materials, including (a) high film purity, (b) uniformity over a large surface area, (c) high deposition speed, (d) high coating adhesion strength, and (e) the ability to coat even heat-sensitive substrates [29]. Accordingly, we previously utilized magnetron sputtering to fabricate a strontium titanate thin film on PEEK [30]. Strontium (Sr), an alkaline earth metal in the same group as calcium (Ca), promotes osteoblast differentiation, and its systemic administration reportedly enhance bone formation and inhibit bone resorption [31, 32]. Owing to complications related to cardiovascular disease associated with Sr systemic use [33, 34] current investigations have been focused into its application as a surface-modifying material for implants. Previous studies have reported enhanced bone formation effects through Sr modifications on PEEK and titanium surfaces using PVD and wet coating methods [35–38]. By using strontium titanate, it is possible to simultaneously modify surfaces with titanium, which has bone affinity, and strontium, which promotes bone formation. Despite the potential advantages of strontium titanate modifications, there are very few reports on the modification of PEEK with strontium titanate thin films [39]. Systematic evaluations of material properties, cellular responses, and osteogenic activity in both in vitro and in vivo settings remain insufficient, limiting our understanding of their full potential in biomedical applications. Furthermore, since strontium titanate thin films contain both titanium and strontium, a direct comparison with titanium thin films fabricated on PEEK under the same process conditions is essential to fully elucidate their osteogenic activity.

Therefore, in this study, we aimed to enhance the osseointegration capability of PEEK by modifying its surface with strontium titanate using magnetron sputtering technology. We fabricated PEEK modified with titanium and strontium titanate and systematically compared the osteogenic activity of three groups: unmodified PEEK (PEEK), titanium-modified PEEK (PEEK-Ti), and strontium titanate-modified PEEK (PEEK-STO). Through in vitro and in vivo experiments, we evaluated the effects on osteoblast differentiation, mineralization, and osseointegration, exploring the potential application of PEEK-STO in orthopedic and spinal implants.

2 Materials and methods

2.1 Material preparation

We obtained PEEK samples from Daipra Corporation Osaka, Japan, through milling processes. For in vitro experiments, cylindrical discs of PEEK measuring 12 mm in diameter and 1 mm in height were used. For in vivo experiments, rectangular prisms of PEEK with dimensions of 2 mm in length, 4 mm in width, and 1 mm in height were used. The sample surfaces were cleaned with ethanol and then dried before deposition.

A magnetron sputtering system (SCV-700LRF, Sanyu Electron, Tokyo, Japan) with an RF generator (13.56 MHz) was used to deposit the film on PEEK samples. The sputtering deposition was carried out using a strontium titanate

($SrTiO_3$) (Toshima Manufacturing, Saitama, Japan) target or a Ti target with dimensions of ϕ 52.1 mm × h 0.5 mm. The samples were placed on a sample holder (ϕ 60 mm), positioned approximately 70 mm from the target. The chamber was initially evacuated to 8 Pa using a rotary pump and further evacuated to a base pressure of around 3×10^{-4} Pa using a turbo-molecular pump. The deposition process was performed at a working pressure of 0.2 Pa, power of 50 W, and argon (Ar) gas flow rate of 8 sccm. The deposition lasted 60 min, and the substrate temperature was maintained near room temperature without heating the sample holder. For in vitro testing, the samples were modified on one side, whereas for in vivo testing, samples were modified on both sides.

2.2 Material characterization

The surface morphology of PEEK, PEEK-Ti, and PEEK-STO was measured using a scanning electron microscope (S-4800, Hitachi High-Technologies, Tokyo, Japan).

The surface chemical states were analyzed using X-ray photoelectron spectroscopy (XPS, ESCA 3057; Ulvac-PHI, Inc.) with monochromatic Al-Kα X-rays (photon energy 1486.6 eV) at 14 kV and 200 W. The samples were placed on a sample holder and introduced to a high vacuum with an initial pressure of approximately 10^{-9} Torr. A charge neutralizer was employed during the analysis.

The pass energies for the survey spectra and element core-level spectrum were 94 eV and 24 eV, respectively. Spectra analysis was performed using Shirley's background subtraction method in CasaXPS software (n = 3/group).

The wettability of the PEEK surfaces was assessed by measuring the water contact angle (WCA) using an automatic contact angle meter (DropMaster300, Kyowa Interface Science, Saitama, Japan). Ultrapure water (3 µL droplets) was deposited in three different areas on each sample (n = 3/group), and images of the droplets on the surface were captured with a camera after 1 s.

The microscopic surface roughness of the materials was measured using a 3D laser scanning microscope (VR-6000, Keyence, Osaka, Japan) (n = 3/group).

2.3 Release of Sr ion

PEEK-STO was immersed in 3 mL of PBS at 37 °C. All solutions were collected at 1, 3, 5, 7, 10, and 14 day intervals and transferred to fresh PBS. The amount of Sr ions in the collected PBS was measured using ICP-AES (Shimadzu, Kyoto, Japan). This experiment was performed in triplicate.

2.4 Cytocompatibility in vitro

2.4.1 Isolation and culture of cells

The experiments used compact bone-derived mesenchymal stromal cells (CB-MSCs) and calvarial osteoblasts. The cells were isolated and cultured according to previously published protocols [40, 41]. Briefly, for the isolation of CB-MSCs, 4-week-old C57BL/6 J mice were sacrificed using CO2, and the femurs and tibias were excised. After removing the bone ends, the bone marrow was flushed using a 27-gauge needle and syringe. The compact bone tissue was cut into 1–3 mm fragments with scissors and then incubated with 0.25% collagenase type 2 (FUJIFILM Wako Pure Chemical, Osaka, Japan) for 2 h. Subsequently, the bone chips were seeded into 10 cm dishes containing growth medium composed of α-MEM (Nacalai Tesque, Kyoto, Japan) supplemented with 10% fetal bovine serum (Sigma-Aldrich, St. Louis, MO, USA) and 1% antibiotic–antimycotic solution (Sigma-Aldrich, St. Louis, MO, USA). Adherent cells were collected 5 days later. Cells from the third passage were used for the following experiments.

To isolate calvarial osteoblasts, 3-day-old C57BL/6 J mice were sacrificed using CO2, and the calvaria were excised. After removing the soft tissues, the calvaria chopped into small pieces were incubated in a digestion solution containing trypsin and collagenase type 2. This process was repeated four times, and the cell suspensions from the last two digestions were cultured in dishes containing the growth medium. Cells from the third passage were used for the following experiments.

2.4.2 Cell proliferation test on material surface

Cell proliferation was assessed using the WST-8 assay (Cell Count Reagent SF, Nacalai Tesque, Kyoto, Japan). Approximately 3×10^4 CB-MSCs were seeded onto each PEEK disk in a 24-well plate and incubated in 1 mL of growth medium at 37 °C (n = 3/group). After 1, 4, 7, and 10 days of incubation, the WST-8 reagent was added to each well and further incubated at 37 °C for 2 h. The absorbance of each well was measured at 450 nm using a microplate reader (Multiskan GO, Thermo Fisher Scientific, Waltham, MA, USA).

2.4.3 Indirect cytotoxity test

All samples were incubated in growth medium at a ratio of 1 mL per 3 cm^2 under standard cell culture conditions for 72 h, according to the protocol outlined in ISO 10993–12, and the extract was subsequently collected. CB-MSCs were seeded into a 96-well plate at a density of 2000 cells per well and incubated for 24 h under standard cell culture

conditions. The medium was then removed, and 100 µL of the sample extract was added, followed by further incubation for either 24 or 72 h ($n=4$/group). As a negative control, cells were cultured in medium that had not been in contact with the samples. As a positive control, cells were cultured with extracts of brass wires. The WST-8 reagent was added to each well and incubated for an additional 2 h at 37 °C. The absorbance was then measured at 450 nm using a microplate reader. Cell viability was calculated as a percentage relative to the negative control, and the cytotoxicity assessment was conducted according to ISO 10993-5.

2.4.4 Cell adhesion and morphology

Approximately 3×10^4 CB-MSCs were seeded onto each PEEK disk in a 24-well plate and incubated in 1 mL of growth medium at 37 °C ($n=3$/group). After 60 min of incubation, the cells were washed three times with PBS. Subsequently, the cells were fixed with 4% paraformaldehyde solution for 10 min, permeabilized with 0.3% Triton X-100 for 15 min, and the nuclei were stained with Nuclear Red™ DCS1 (AAT Bioquest, Pleasanton, CA, USA) for 30 min. The cells were washed three more times with PBS to remove background staining. The cells' adhesion status was analyzed using a fluorescence microscope (FM1200 NIKON, Tokyo, Japan), with five random fields of view selected from the center and four directions. Cell counts were acquired using Image J software (National Institutes of Health, Bethesda, MD, USA). When observing cell morphology, cells were fixed 24 h after seeding. Alexa Fluor™ 488 Phalloidin (Thermo Fisher Scientific, Waltham, MA, USA) staining of the actin cytoskeleton was added in the dark for 1 day before nuclear staining.

2.5 Osteogenic activity

2.5.1 Alkaline phosphatase activity assay

CB-MSCs were seeded onto each PEEK disk at a density of 3×10^4 in growth medium and, after 1 day, were cultured in osteogenic medium (αMEM containing 10% FBS, 1% penicillin-streptomycin, 50 µg/mL L-ascorbic acid, 10 mM β-glycerol phosphate, 10 nM dexamethasone) ($n=3$/group).

Table 1 Primers for qPCR

Genes	Forward (5'−3')	Reverse (5'−3')
Alp	AGCGACACGGACAAGAAGC	GGCAAAGACCG CCACATC
Ocn	GCAATAAGGTAGTGAACAGA CTCC	CCATAGATGCGT TTGTAGGCGG
Bsp	AATGGAGACGGCGATAGTTC CG	GGAAAGTGTGG AGTTCTCTGCC
Gapdh	AGGTCGGTGTGAACGGATTTG	TGTAGACCATGT AGTTGAGGTCA

ALP activity was measured on day 7 or day 14 after osteogenesis induction using the ALP assay kit (LaboAssay™ ALP, FUJIFILM Wako Pure Chemical) following the manufacturer's protocol. One unit of enzyme activity was defined as the amount of enzyme that catalyzes the conversion of 1 nmol of p-nitrophenol per minute at pH 9.8 and 37 °C. The activity was normalized to the protein content, determined using the BCA Protein Assay Kit (Pierce™, Thermo Fisher Scientific). ALP activity on PEEK-Ti and PEEK-STO was calculated relative to PEEK.

2.5.2 RT-qPCR

CB-MSCs were cultured on each PEEK in osteogenic medium for 7 and 14 days in a 24-well plate ($n=3$/group). The cells were homogenized with TRIzol Reagent (Thermo Fisher Scientific, Waltham, MA, USA). Total RNA was extracted using the Direct-zol RNA kit (Zymo Research, Orange, CA, USA) and reverse-transcribed to cDNA using ReverTra Ace qPCR RT Master Mix (Toyobo, Osaka, Japan). Gene expression was measured using real-time PCR with SYBR Green Master Mix (Applied Biosystems, Foster City, CA, USA) in Step One Plus Real-Time PCR System (Applied Biosystems). Target gene expression levels were normalized to those of *Gapdh*, and fold changes were calculated relative to the control group (PEEK) using the $2-\Delta\Delta Ct$ method. The primer sequences are shown in Table 1.

2.5.3 Quantification of mineralization and Ca deposition

Mineralization was assessed after 21 days of culture of CB-MSCs and calvarial osteoblasts in the osteogenic medium (n=3/group). The cultured cells were washed twice with PBS and fixed with 4% PFA for 20 min. After washing twice with PBS, the matrix mineralization was stained with Alizarin Red solution (Mutoh Chemical, Tokyo, Japan) for 30 min and dissolved with 5% formic acid. The absorbance of the solution was measured at 415 nm to quantify the mineralization. Since Sr is known to react with Alizarin red, it may overestimate mineralization by osteoblasts [42]. Therefore, the concentration of Ca in the solution was also measured using ICP-AES. The Ca precipitation on the samples was calculated from the Ca concentration.

2.6 SBF assay

To verify the mineral deposition potential by non-cellular mechanisms, samples were immersed in a simulated body fluid (SBF) solution without cells. The SBF solution and the volume used during the test were prepared and calculated according to the protocol formulated by Kokubo et al. [43]. Each sample was immersed in SBF for 28 days. After

immersion, each sample was carefully washed with distilled water and dried at room temperature. The surfaces were observed using SEM.

The distribution of the precipitated calcium phosphate was measured using time-of-flight secondary ion mass spectrometry (TOF-SIMS) ($n=3$/group). TOF-SIMS analysis was performed with a TOF-SIMS M6 instrument (ION-TOF GmbH, Münster, Germany) using a Bi_3^+ cluster ion gun as the primary ion source. Spectrums ranging from 500 × 500 µm were analyzed using a pulsed primary ion beam (Bi_3^+, 0.42pA at 30 keV), with a 295-s acquisition time. Positive and negative spectra were recorded for each specimen. The secondary ion peaks' mass resolution (m/Δm) was typically between 5000 and 9000. The mass scale for the positive secondary ions was calibrated using the CH^+, $C_2H_2^+$, and $C_3H_3^+$ peaks. The negative secondary mass scale was calibrated using the C^-, $C2^-$, and $C3^-$ peaks. The observation of characteristic TOF-SIMS peaks was limited to the mass range of 1 to 100 D in both positive and negative spectra. To detect the relative precipitation of calcium phosphate, Ca^+ was measured in positive ion mode, and phosphate fragments (PO_2^-, PO_3^-) were measured in negative ion mode. Each ion intensity of PEEK-Ti and PEEK-STO was calculated relative to PEEK.

2.7 In vivo assay

2.7.1 Animals and surgical procedures

The Animal Experiment Committee of our institution approved all animal surgeries. Twelve 12-week-old SD rats ($n=4$/group) were purchased from Jackson Laboratory Japan (Kanagawa, Japan). Anesthesia was induced with a mixture of 0.15 mg/kg medetomidine, 2.0 mg/kg midazolam, and 2.5 mg/kg butorphanol administered intraperitoneally. After making an incision on the lateral side of the right knee, the patella was dislocated medially to expose the femoral articular surface. A cortical window (1 × 2 mm) was created in the intercondylar region using a diamond burr with 1 mm diameter. The entire length of each sample for in vivo use was inserted into the distal bone marrow through the cortical window. The rats were allowed free access to water and food postoperatively. They were sacrificed with CO2 at 4 weeks post-surgery. Micro-focus computed tomography (micro-CT) and histological analysis were performed to evaluate bone formation around the implant.

2.7.2 Micro-CT

The collected samples were preserved in 70% ethanol and subjected to micro-CT scanning (Skyscan 1272 micro-CT, Bruker, Kontich, Belgium) with the following parameters: camera binning = 2 × 2, power voltage = 80 kV, power current = 125 µA, image pixel size = 5 µm, rotation step = 0.6°, filter = Al 1 mm. Image analysis was performed using CTAN software (version 1.18.8.0 +, Bruker).

2.7.3 Histological evaluation

The extracted samples were fixed in 70% ethanol, treated with Villanueva bone stain, and then embedded in methacrylate. Polished sections in the coronal plane were prepared, and images of the sections were captured using an optical microscope's 10 × objective lens (BZ-800, Keyence, Osaka, Japan). The bone-implant contact ratio (BIC%) was calculated by dividing the direct bonding distance between the implant surface and bone tissue by the overall distance. Furthermore, the proximity zone up to 20 µm from the implant surface was set as ROI-I, while the distant zone from 20 µm to 60 µm was set as ROI-II. The bone area ratio (BA%) was calculated by measuring the bone area within each zone and dividing by the total area of each zone.

2.8 Statistical analysis

Data are expressed as mean ± standard deviation, and multiple comparisons were performed among all groups using Tukey's HSD test after one-way analysis of variance (ANOVA). Analysis was performed using GraphPad Prism 10.1.2, with p-value < 0.05 considered statistically significant (*$p<0.05$, **$p<0.01$, ***$p<0.001$, ****$p<0.0001$).

3 Results

3.1 Material characterization

SEM observations revealed changes in the surface morphology at both the micro and nano levels in PEEK-Ti and PEEK-STO compared to PEEK (Fig. 1a). XPS analysis confirmed surface modifications with titanium and strontium titanate on the PEEK surface (Fig. 1b). The atomic concentration ratios of each sample are shown in Fig. 1c. The water contact angle of the material increased in the order of PEEK, PEEK-STO, and PEEK-Ti, and the wettability was not improved by the deposition of the thin films (Fig. 2a). Surface roughness measurements using a 3D laser scanning microscope showed significant surface flattening in the PEEK-Ti group compared to the PEEK and the PEEK-STO groups (Fig. 2b).

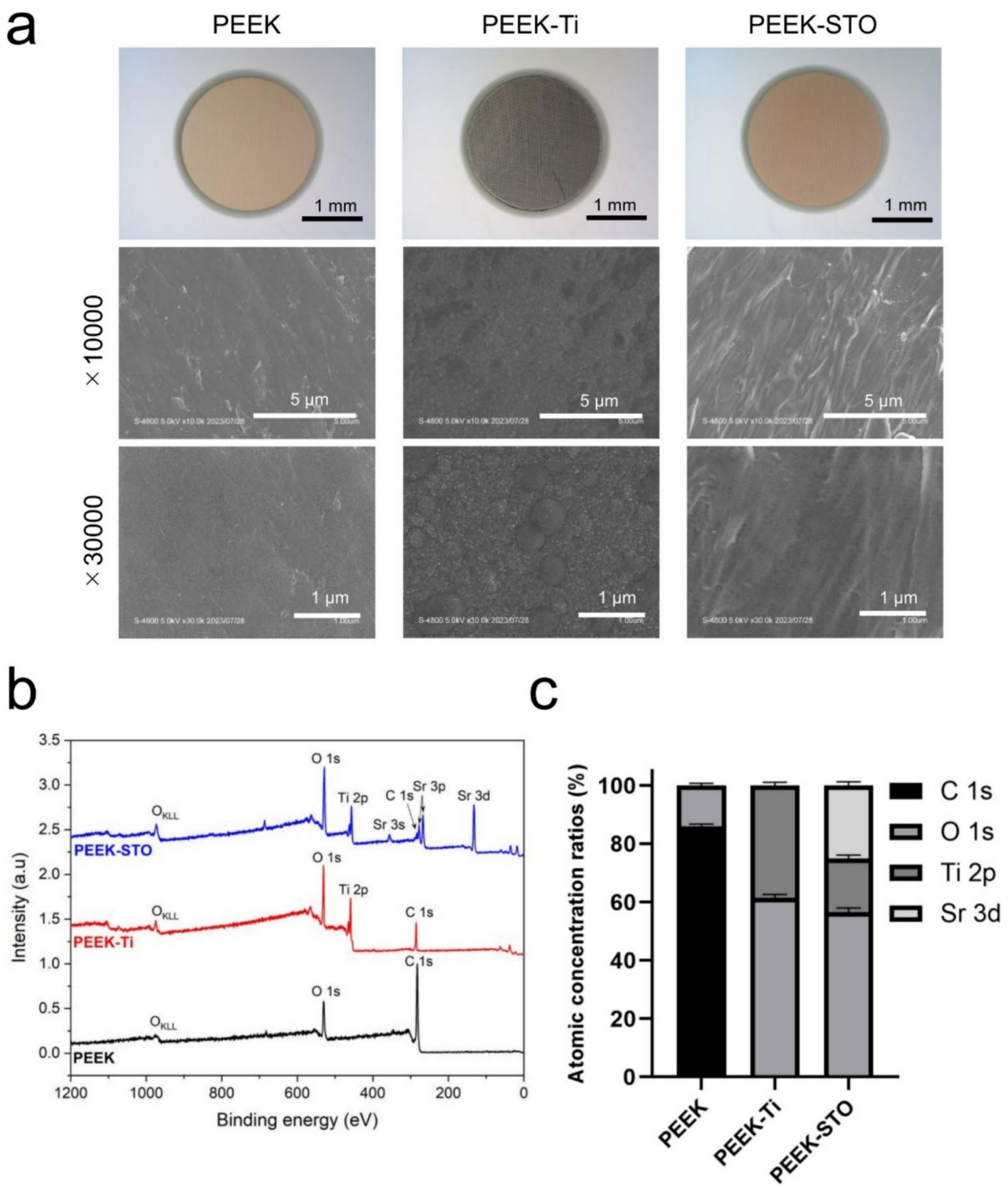

Fig. 1 Material characterization (SEM, XPS). (**a**) Photomicrographs (top) and SEM images of PEEK, PEEK-Ti, and PEEK-STO: magnification = × 10000 (middle), × 300000 (bottom). (**b**) Representative XPS spectra for each sample. (**c**) Atomic concentration ratios of the surface of each sample measured by XPS ($n = 3$). Data represent mean ± SD (error bars)

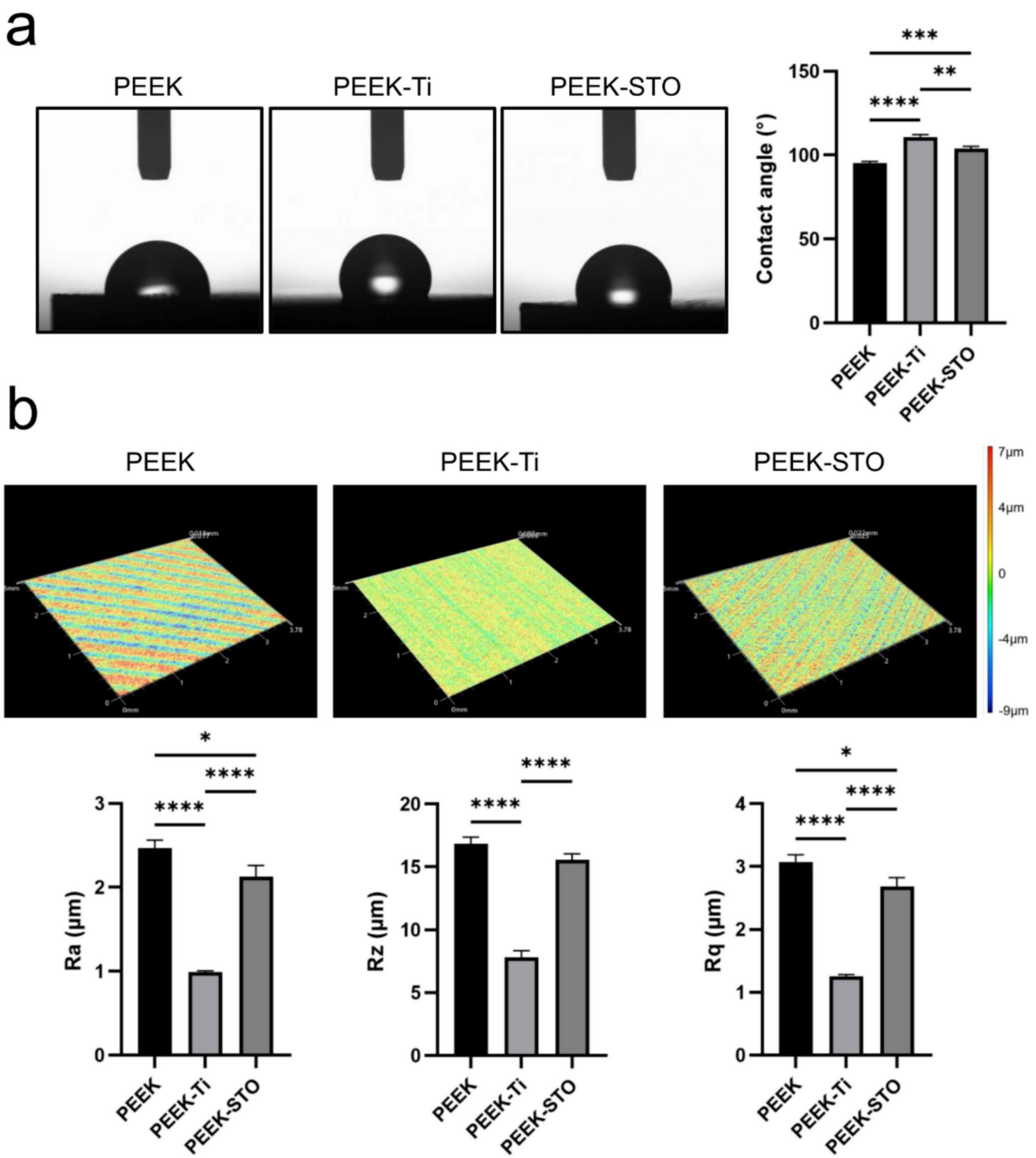

Fig. 2 Material characterization (WCA, roughness). (**a**) Water contact angle of PEEK, PEEK-Ti, and PEEK-STO ($n=3$). (**b**) Microroughness of PEEK, PEEK-Ti, and PEEK-STO evaluated by 3D laser scanning ($n=3$). Data represent mean ± SD (error bars). *$p<0.05$, **$p<0.01$, ***$p<0.001$, ****$p<0.0001$ by one-way ANOVA followed by Tukey's HSD test

3.2 Release of Sr ion

In the Sr release kinetics analysis, most of the Sr was released from PEEK-STO within the first 3 days (Fig. 3). The total amount of released Sr was 36.7 ± 0.8 μg.

3.3 Cytocompatibility in vitro

Cell viability on PEEK, PEEK-Ti, and PEEK-STO was measured using CB-MSCs. Both PEEK-Ti and PEEK-STO showed no decrease in cell viability compared to PEEK (Fig. 4a). On days 1 and 3 of culture, CB-MSCs were more viable on PEEK-STO than on PEEK. However, this difference disappeared by day 7. In the cytotoxicity test using extracts of the materials, cell viability exceeded 80% in all samples, demonstrating no cytotoxicity in accordance with ISO 10993–5 criteria. The number of adherent cells at 60 min after seeding did not differ among the three groups (Fig. 4b), and the cell adhesion morphology showed similar actin fiber spreading among the three groups at 24 h after seeding (Fig. 4c).

3.4 Osteogenic activity

The protocol for assessing osteogenic activity in vitro is shown (Fig. 5a). In the evaluation of osteogenic activity using ALP analysis, PEEK-STO showed the highest ALP activity on day 7 after osteogenesis induction. On day 14, both PEEK-Ti and PEEK-STO exhibited higher ALP activity compared to PEEK (Fig. 5b). Gene expression analysis showed that *Alp*, which reflects osteoblast activity, as well as the non-mineralized bone matrix components *Ocn* and *Bsp* of PEEK-STO were significantly higher compared to PEEK and PEEK-Ti on day 7 after osteogenesis induction.

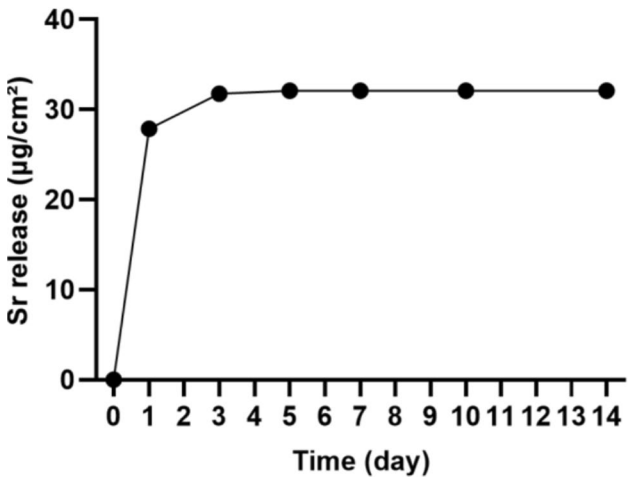

Fig. 3 Sr release kinetics. The amount of strontium released from PEEK-STO up to day 14 ($n=3$), the error bars are smaller than the sizes of symbols

Subsequently, the expression of osteogenesis-related genes in PEEK-Ti also increased, and by day 14, the difference between PEEK-Ti and PEEK-STO had disappeared (Fig. 5c). The increase in ALP activity and the expression of osteogenesis-related genes in PEEK-STO on day 7 may be attributed to Sr release, while the similar increase in osteogenic activity of both PEEK-Ti and PEEK-STO on day 14 may be due to the bone affinity of the titanium-containing thin film. On day 21, the mineralization of the extracellular matrix and Ca content was evaluated by Alizarin Red staining and ICP-AES, respectively. PEEK-STO showed significantly greater staining with Alizarin Red and Ca deposition (Fig. 6a, b, and c). These results indicate that PEEK-STO enhances early osteogenic differentiation and mineral deposition.

3.5 Verification of mineral deposition by non-cellular mechanisms using SBF

SEM images of PEEK immersed in SBF for 28 days showed no apparent accumulation of hydroxyapatite crystals in all groups (Fig. 7a). The TOF–SIMS assay to detect precipitated calcium phosphate showed a significant increase in calcium phosphate precipitation for PEEK-Ti and PEEK-STO compared to PEEK. This result indicates that both PEEK-Ti and PEEK-STO have comparable non-cellular calcium phosphate precipitation capacity (Fig. 7b). High-resolution TOF-SIMS spectra in positive and negative ion modes for PEEK, PEEK-Ti, and PEEK-STO are shown (Fig. S1).

3.6 In vivo assay

Subsequently, an in vivo implantation assay was conducted to evaluate the materials' osteogenic activity. The protocol for assessing osteogenic activity in vivo is shown (Fig. 8a). PEEK is radiolucent, allowing for the evaluation of bone formation on the surface of implants by micro-CT. Micro-CT image analysis 4 weeks after the implantation showed that new bone had formed over the entire surface of the PEEK-STO. On the other hand, the bone formation around the PEEK and PEEK-Ti was less continuous than that of the PEEK-STO (Fig. 8b).

Histological evaluation of hard tissue sections showed that PEEK-STO showed bone formation on the implant surface without fibrous tissue interposition (osseointegration). In contrast, PEEK showed the intervening fibrous tissue between PEEK and newly formed bone. PEEK-Ti also showed bone formation on the implant surface without the intervention of fibrous tissue, but the area of bone covering PEEK-Ti was smaller than that of PEEK-STO (Fig. 9a). A description of the zone setting around implants for bone area ratio measurements is shown (Fig. 9b). Bone-to-implant

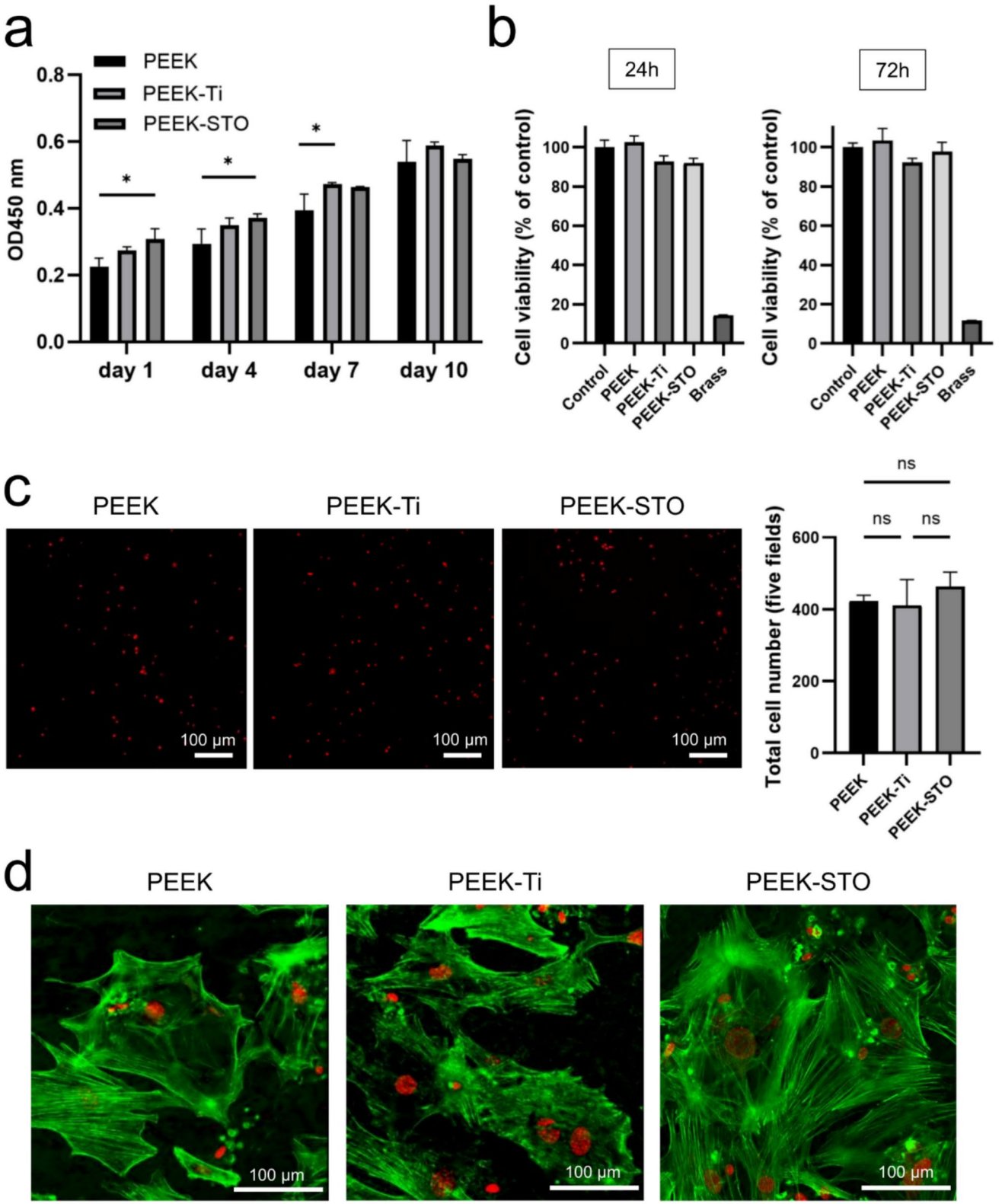

Fig. 4 Cytocompatibility in vitro. (**a**) Proliferation of CB-MSCs on PEEK, PEEK-Ti, and PEEK-STO on days 1, 4, 7, and 10 after seeding. (**b**) Cell viability after culturing CB-MSCs for 24 or 72 h with extracts of PEEK, PEEK-Ti, and PEEK-STO. Control**:** Growth medium not in contact with the test samples. Brass**:** Extract of brass wires. (**c**) Confocal laser microscope images and the total number of adhered cells in five fields of view for PEEK, PEEK-Ti, and PEEK-STO after 1 h of cell seeding: Nuclear red for cell nuclei (red). (**d**) Actin cytoskeleton of cells on PEEK, PEEK-Ti, and PEEK-STO after 24 h of seeding: Nuclear red for cell nuclei (red), phalloidin for actin filaments (green). Data represent mean ± SD (error bars). *$p < 0.05$ by one-way ANOVA followed by Tukey's HSD test. ns: not statistically significant

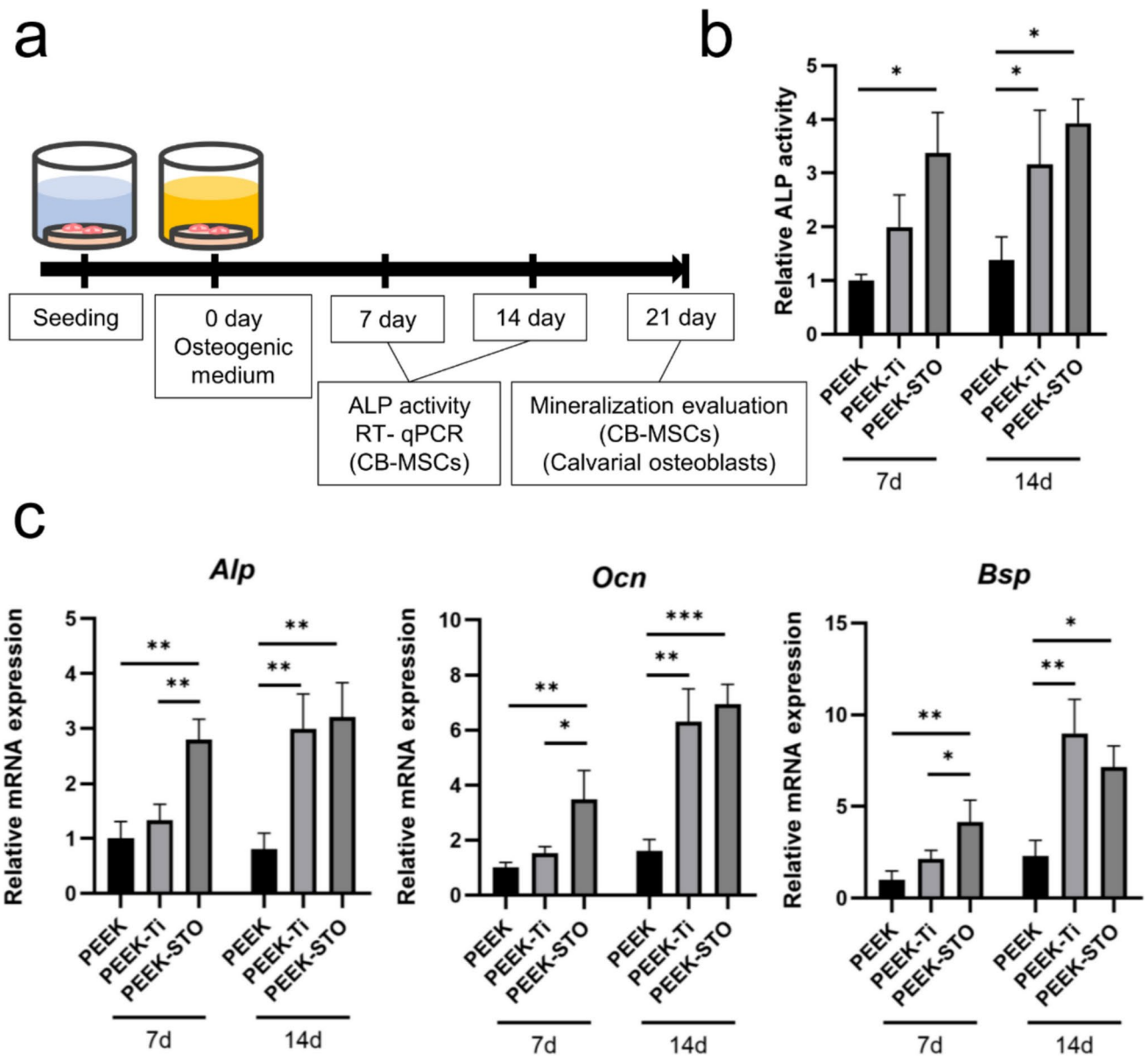

Fig. 5 Osteogenic activity (ALP activity, gene expression). (**a**) Schematic of the protocol for the osteogenic activity experiment. (**b**) Relative ALP activity of CB-MSCs treated with the osteogenic medium on PEEK, PEEK-Ti, and PEEK-STO. (**c**) Relative osteogenic activity-related gene expression of CB-MSCs treated with osteogenic medium on PEEK, PEEK-Ti, and PEEK-STO. Data represent mean ± SD (error bars). *$p<0.05$, **$p<0.01$, ***$p<0.001$ by one-way ANOVA followed by Tukey's HSD test

contact ratio (BIC%) and bone area ratio (BA%) in the proximity zone from the implant (ROI-I) were significantly larger in PEEK-STO (BIC%: 69.0 ± 12.4, BA%: 50.6 ± 3.6) compared to PEEK-Ti (BIC%: 46.6 ± 6.3, BA%: 36.5 ± 4.8) and PEEK (BIC%: 11.9 ± 5.5, BA%: 22.0 ± 9.3) at 4 weeks after surgery (PEEK-STO vs PEEK-Ti; $p<0.05$, PEEK-STO vs PEEK; $p<0.01$). The bone area ratio in the distant zone from the implant (ROI-II) did not significantly differ among the three groups (Fig. 9c, d, and e). These results suggest that PEEK-STO enhances bone formation near the implant and could achieve the highest osseointegration around the implant.

4 Discussion

In this study, we compared the osteogenic activity and osseointegration capacity among PEEK, PEEK-Ti, and PEEK-STO. PEEK-STO significantly enhanced the early expression of osteogenic genes and alkaline phosphatase (ALP) activity of CB-MSCs compared to PEEK and

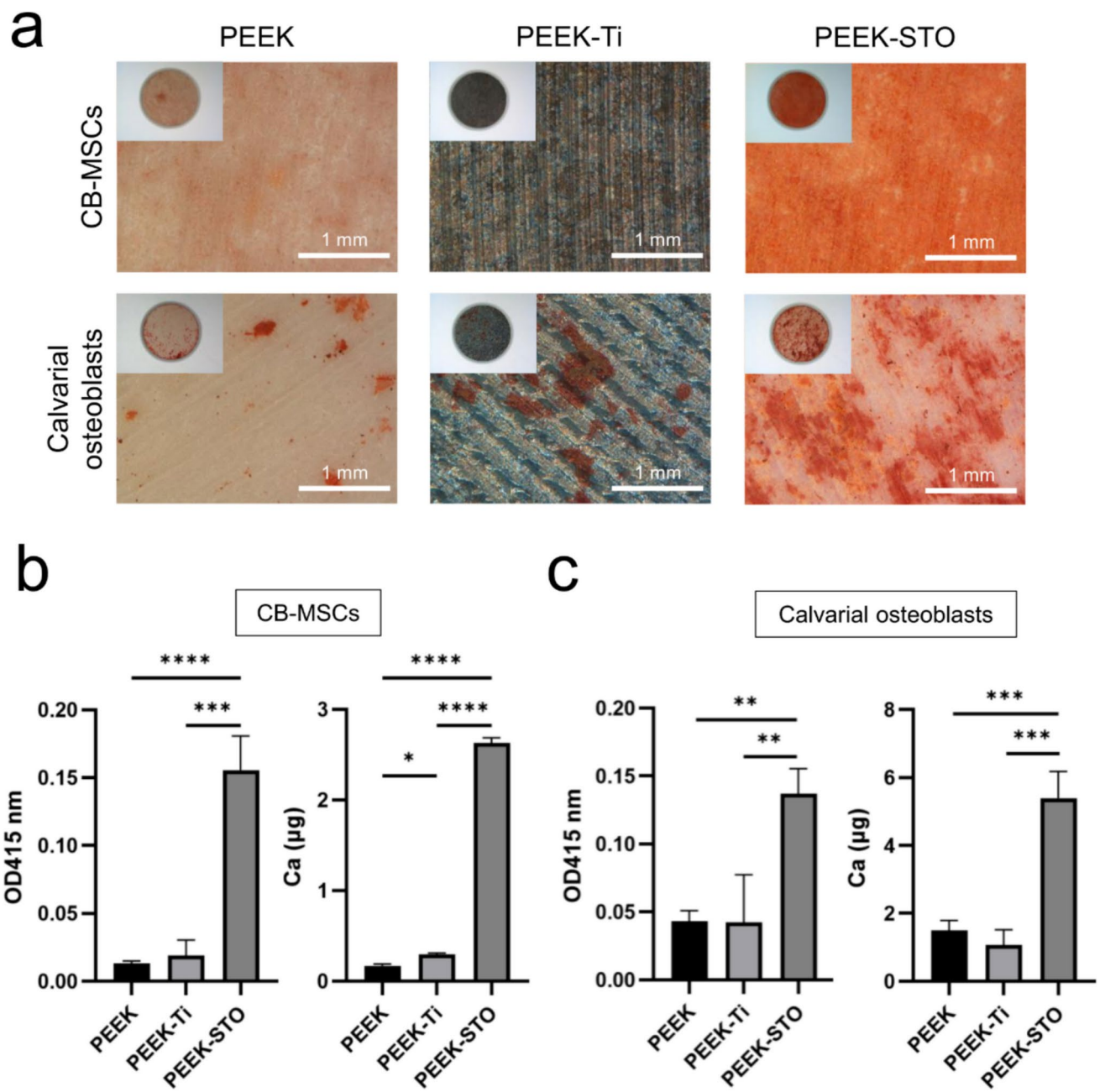

Fig. 6 Osteogenic activity (mineralization). (**a**) Photomicrographs of PEEK, PEEK-Ti, and PEEK-STO after Alizarin Red staining. The upper panel shows CB-MSCs, and the lower panel shows calvarial osteoblasts. (**b**) Absorbance of Alizarin Red eluate and Ca content measured by ICP-AES in CB-MSCs. (**c**) Absorbance of Alizarin Red eluate and Ca content measured by ICP-AES in calvarial osteoblasts. Data represent mean ± SD (error bars). $*p<0.05$, $**p<0.01$, $***p<0.001$, $****p<0.0001$ by one-way ANOVA followed by Tukey's HSD test

PEEK-Ti, ultimately leading to the highest calcium deposition among them. The simulated body fluid (SBF) test, which investigates mineral deposition by non-cellular mechanisms, showed enhanced calcium phosphate deposition in both PEEK-STO and PEEK-Ti compared to PEEK. In vivo analysis using a rat femur implantation model demonstrated that PEEK-STO has the strongest osteointegration capacity among the groups. This enhanced osseointegration capacity of PEEK-STO is likely attributed to the following characteristics.

Notably, Sr ions released from PEEK-STO might exert osteogenic effects. The Sr solubility of high-crystalline strontium titanate in aqueous solution is very low, less than 3% of the total amount for 7 days, even for fine particles [44, 45]. The release kinetics are also different: crystalline strontium titanate is released at a nearly constant rate, whereas amorphous or low-crystalline strontium titanate

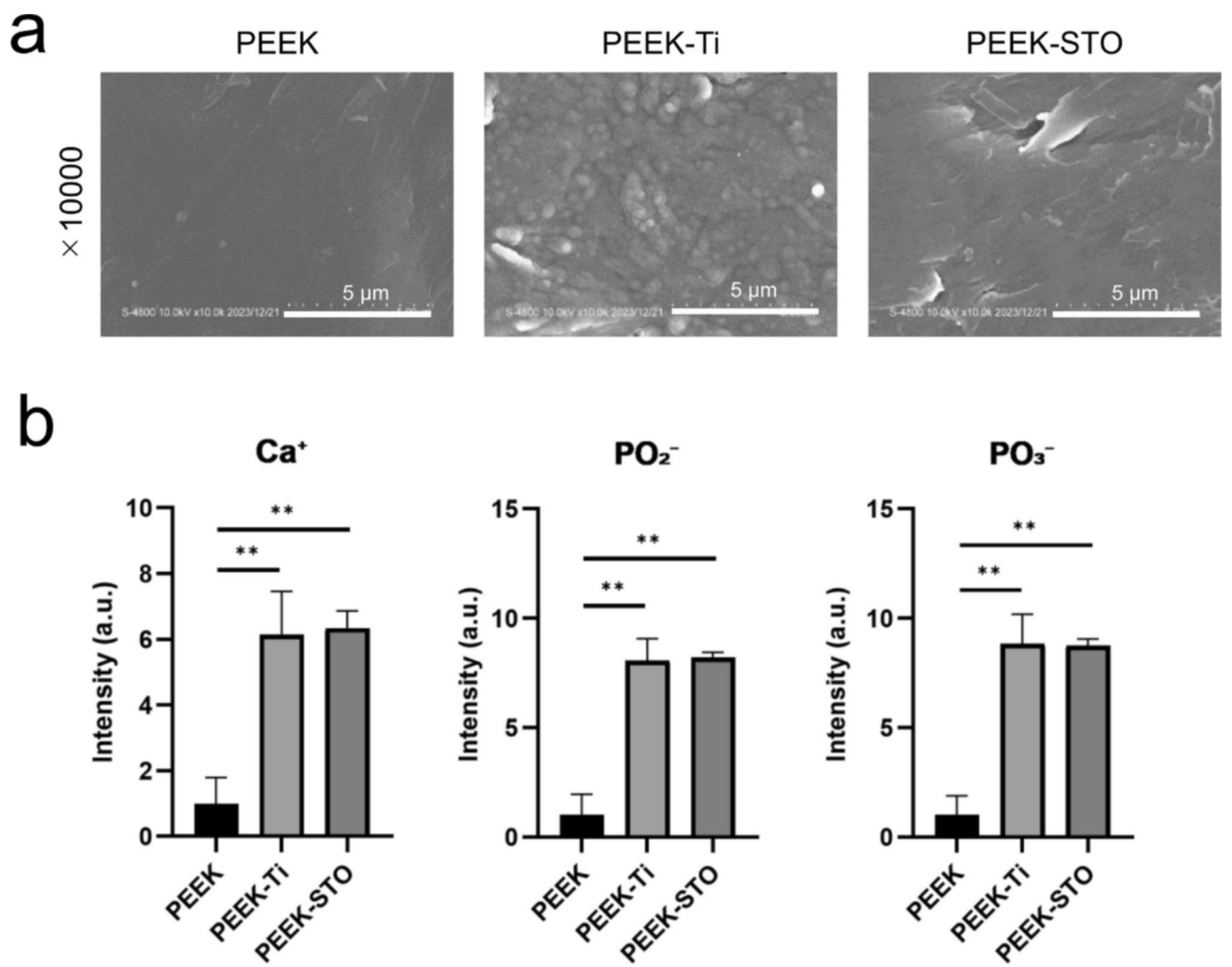

Fig. 7 SBF assay. (**a**) SEM images of PEEK, PEEK-Ti, and PEEK-STO after SBF soaking: magnification = × 10000. (**b**) Intensity ratio of Ca^+ ions and phosphate fragment ions (PO_2^-, PO_3^-) measured by TOF-SIMS. Data represent mean ± SD (error bars). $^{**}p < 0.01$ by one-way ANOVA followed by Tukey's HSD test

has the highest initial release followed by an exponential decay [35, 46, 47]. The release kinetics of Sr in this study are also consistent with those of amorphous or low-crystalline strontium titanate, because most of the Sr was released in the initial phase and decayed exponentially. Based on the thin film formation efficiency using strontium titanate as the target material in our apparatus and Sr atomic concentration in the XPS, the total Sr content of the thin film can be estimated to be approximately 83 μg [30]. The percentage of Sr released from the thin film in this experiment was approximately 45%, higher than that of high-crystalline strontium titanate. The total amount of strontium released was 36.7 ± 0.8 μg, corresponding to a concentration < 0.5 mM in 1 mL of the medium. This concentration is within the range of concentrations where Sr promoted osteogenic activity (0.01–1 mM) [48–50].

Furthermore, PEEK-STO has the potential to deposit calcium phosphate on the surface by non-cellular mechanisms. Titanium reportedly deposits calcium phosphate in simulated body fluid (SBF), which is considered a factor contributing to its osteoconductivity [51]. In this study, PEEK-STO deposited a calcium phosphate layer in SBF comparable to that of PEEK-Ti. The 2–5 nm titanium oxide film on titanium is known as a passive film and has an amorphous or low-crystalline structure, and calcium phosphate is deposited on the titanium oxide film in SBF [51–53]. Phosphate ions are first absorbed on the titanium oxide film and then stabilized on the film by combining with Ca ions to form calcium phosphate [51]. Calcium and phosphorus exist at the interface between titanium and bone tissue and may contribute to osseointegration of titanium [54, 55]. Following the above process, titanium oxide formed on PEEK-STO

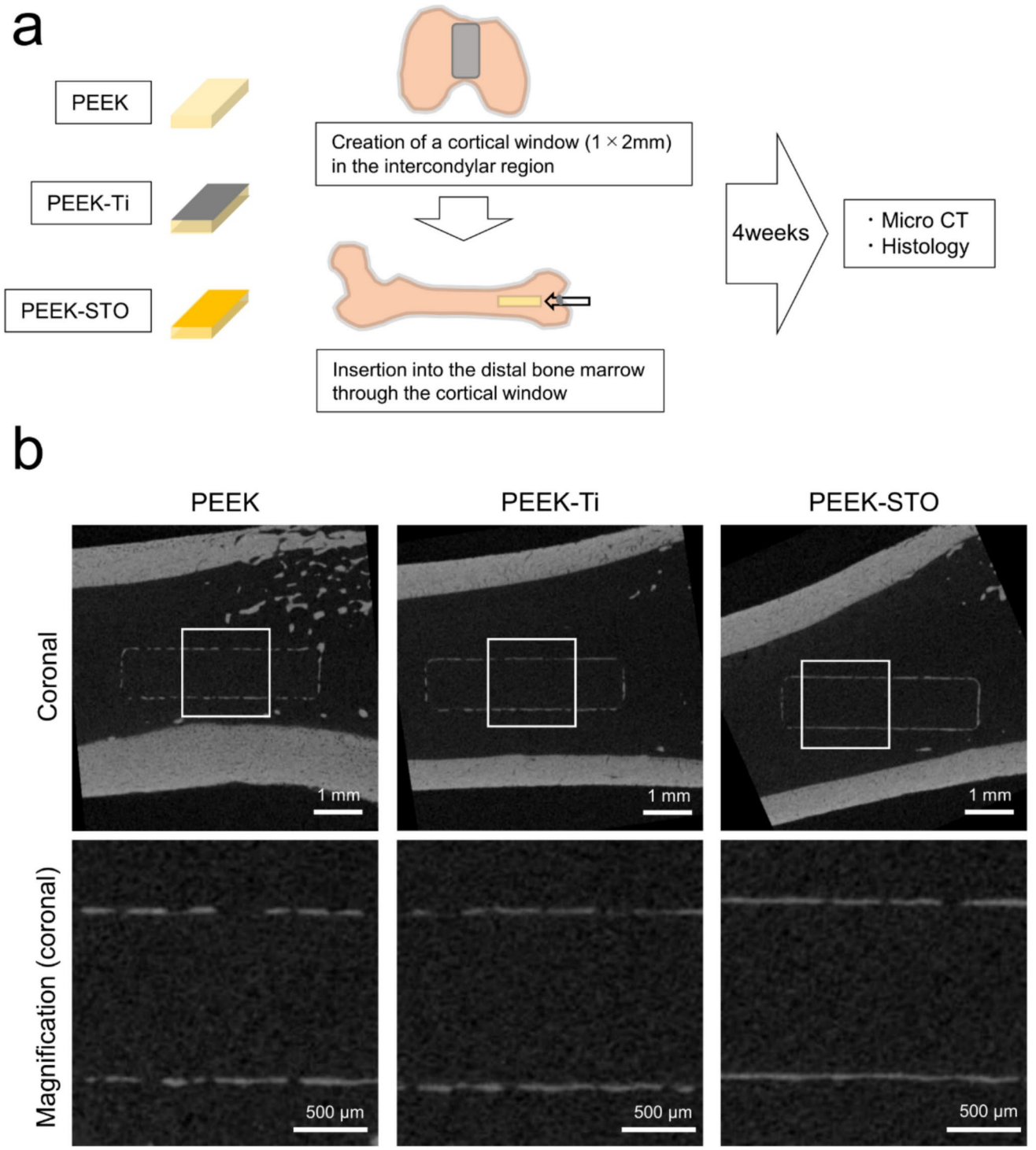

Fig. 8 In vivo assay (micro-CT). (**a**) Schematic of the in vivo experiment protocol. (**b**) Representative micro-CT images: Coronal (upper), magnified coronal view (lower)

may have contributed to calcium phosphate deposition and osseointegration.

This study has some limitations. Magnetron sputtering is a technique that simultaneously induces morphological and chemical changes on the material surface, and unintended changes in these properties may have influenced osteogenic activity [46, 56, 57]. Additionally, osseointegration could be optimized by modulating strontium release from the material surface by changing the film thickness and target material composition. Another limitation is that the precise

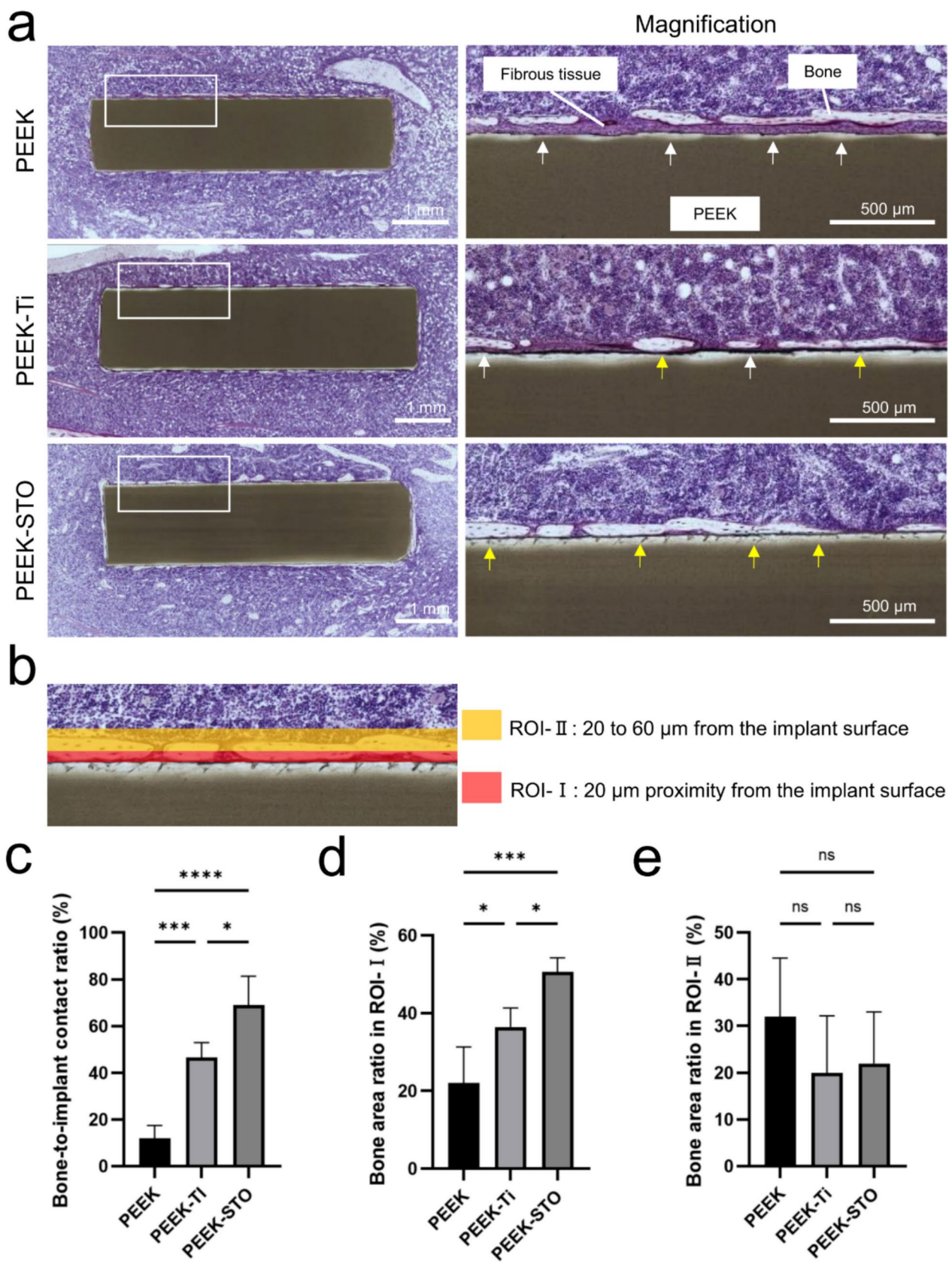
a
Magnification
PEEK
PEEK-Ti
PEEK-STO
Fibrous tissue
Bone
PEEK
1 mm
500 μm
b
ROI-Ⅱ: 20 to 60 μm from the implant surface
ROI-Ⅰ: 20 μm proximity from the implant surface
c
Bone-to-implant contact ratio (%)
****
***
*
d
Bone area ratio in ROI-Ⅰ (%)
***
*
e
Bone area ratio in ROI-Ⅱ (%)
ns
PEEK
PEEK-Ti
PEEK-STO

Fig. 9 In vivo assay (histology). (**a**) Representative images of hard tissue sections (coronal section) of PEEK, PEEK-Ti, and PEEK-STO: low magnification (left), high magnification (right). The white arrows indicate areas where fibrous tissue is interposed between the implant and bone tissue, and the yellow arrows indicate areas where the implant is directly bonded to the bone tissue. (**b**) Description of the zone setting around implants for bone area ratio measurements. (**c**) Bone-to-implant contact ratio (BIC%) of PEEK, PEEK-Ti, and PEEK-STO ($n=4$). (**d**) Bone area ratio in the proximity zone from the implant (ROI-I) ($n=4$). (**e**) Bone area ratio in the distant zone from the implant (ROI-II) ($n=4$). Data represent mean ± SD (error bars). *$p<0.05$, ***$p<0.001$, ****$p<0.0001$ by one-way ANOVA followed by Tukey's HSD test. ns: not statistically significant

molecular mechanisms by which strontium titanate and titanium modifications affect surface properties and cellular responses remain unclear, requiring further investigation. The in vivo evaluation was limited to four weeks, which may be insufficient to assess long-term osseointegration and biocompatibility. A rat femoral implantation model was used, which does not fully replicate the human spinal fusion environment, highlighting the need for studies using an intervertebral fusion model. In addition, the relatively small sample size may limit statistical power and generalizability of findings, requiring larger studies to be conducted under more clinically appropriate conditions.

In conclusion, we demonstrated that surface modification of PEEK with strontium titanate through magnetron sputtering (PEEK-STO) promotes osteoblast differentiation and calcium deposition and can enhance in vivo osteointegration compared to PEEK-Ti and PEEK. These results suggest that surface modification of PEEK with strontium titanate through magnetron sputtering is an attractive option for solving the problems of PEEK's biological inertness while maximizing PEEK's advantages as a spinal fusion device.

Supplementary Information The online version contains supplementary material available at https://doi.org/10.1007/s42247-025-01033-8.

Acknowledgements We would like to express our gratitude to Yoshihiko Morita from Daipla Corporation for assistance with PEEK sample preparation, and to Yukiko Eguchi, Fumiko Hirayama, and Mari Shinkawa from Osaka University for their experimental support. Special thanks go to Yuji Ohkubo for the WCA measurements, and to Akira Oiwa and Nozomu Hayashi for their assistance with plasma sputtering. We also appreciate the support of Tomoaki Mizuno at the Center for Medical Research and Education, Graduate School of Medicine, Osaka University, for SEM observations. We sincerely appreciate the technical support of Nao Eguchi at the Core Facility Center, Osaka University, for ICP-AES and TOF-SIMS analyses. We would like to thank Editage (www.editage.jp) for English language editing.

Authors' contributions Conceptualization: MI, AAH, SH and TK; Methodology: MI, AAH, TI, SH and TK; Formal analysis and investigation: MI, AAH and KF; Writing—original draft preparation: MI and AAH; Writing—review and editing: TK, MB, TF, HH, YU, DT, YK, MF, TF, SO, SH and TK; Resources: AAH, KF, TI; Project administration: SH and TK; Supervision: SO, SH and TK.

Funding Open Access funding provided by Osaka University.
This research was partially supported by the Japan Society for the Promotion of Science (JSPS) Core-to-Core Program JPJSCCA2019002, and the International Joint Research Promotion Program from Osaka University.

Data availability The datasets generated and analyzed in the current study are available from the corresponding author upon reasonable request.

Declarations

Ethics approval All experiments were approved by the Institutional Animal Committee of Osaka University (approval number: 03-081-003) and were conducted in strict accordance with the NIH Guide for the Care and Use of Laboratory Animals (Committee for the Update of the Guide for theUse of Laboratory Animals, 2011), and The study was reported in accordance with the ARRIVE guidelines.

Competing interests The authors have no relevant financial or non-financial interests to disclose.

References

1. B.G. Diebo, F.P. Lafage, R. Schwab, J.A. Smith, A.M. Mundis, E.M. Ames, Lancet **394**, 160–172 (2019). https://doi.org/10.1016/S0140-6736(19)31125-0
2. S.D. Glassman, S. Berven, K. Bridwell, W. Horton, J.R. Dimar, Spine (Phila Pa 1976) **30**, 682–688 (2005). https://doi.org/10.1097/01.brs.0000155425.04536.f7
3. F.J. Schwab, M. Lafage, A. Patel, R. Farcy, Spine (Phila Pa 1976) **38**, E803–E812 (2013). https://doi.org/10.1097/BRS.0b013e318292b7b9
4. H. Zhang, Y. Wang, L. Zhang, M. Li, Y. Xu, X. Zhang, Front. Bioeng. Biotechnol. **10**, 900992 (2022). https://doi.org/10.3389/fbioe.2022.900992
5. A. Warburton, S.J. Girdler, C.M. Mikhail, A. Ahn, S.K. Cho, Neurospine **17**, 101–110 (2020). https://doi.org/10.14245/ns.1938296.148
6. S. Najeeb, Z.K. Bds, S.Z. Bds, M.S.Z. Bds, J. Oral Implantol. **42**, 512–516 (2016). https://doi.org/10.1563/aaid-joi-D-16-00072
7. S.M. Kurtz, J.N. Devine, Biomaterials **28**, 4845–4869 (2007). https://doi.org/10.1016/j.biomaterials.2007.07.013
8. K. Phan, J.A. Hogan, Y. Assem, R.J. Mobbs, J. Clin. Neurosci. **24**, 138–140 (2016). https://doi.org/10.1016/j.jocn.2015.07.017
9. U.K. Dhar, M. Sharma, R. Singh, A. Sood, S. Gupta, R. Kumar, P. Verma, Eur. Spine J. **32**, 957–968 (2023). https://doi.org/10.1007/s00586-023-07530-w

10. J.-H. Tan, C.K. Cheong, H.W.D. Hey, Eur. Spine J. **30**, 1285–1295 (2021). https://doi.org/10.1007/s00586-021-06748-w
11. R. Smeets, T. Stadlinger, A. Schwarz, C. Beck-Broichsitter, F. Jung, F. Ebker, Biomed. Res. Int. **2016**, 6285620 (2016). https://doi.org/10.1155/2016/6285620
12. T. Goto, Clin. Calcium **24**, 265–271 (2014)
13. B. Yuan, W. Cheng, X. Zhang, D. Wang, Y. Zhang, J. Liu, Biomaterials **170**, 116–126 (2018). https://doi.org/10.1016/j.biomaterials.2018.04.014
14. W.R. Walsh, M.H. Pelletier, N. Bertollo, C. Christou, C. Tan, Clin. Orthop. Relat. Res. **474**, 2364–2372 (2016). https://doi.org/10.1007/s11999-016-4994-x
15. W. Yin, X. Li, Y. Gao, Z. Zhang, Y. Wang, Smart Mater. Med. **3**, 20–36 (2022). https://doi.org/10.1016/j.smaim.2021.11.005
16. K. Masamoto, Y. Yamada, M. Hashimoto, H. Fukuda, H. Ohashi, T. Uchida, Acta Biomater. **91**, 48–59 (2019). https://doi.org/10.1016/j.actbio.2019.04.041
17. Y.-S. Chen, L. Xu, S. Zhang, Y. Zhou, X. Yu, Surf. Coat. Technol. **350**, 904–912 (2018). https://doi.org/10.1016/j.surfcoat.2018.03.071
18. Y. Förster, L. Mühleder, A. Ristl, M. Priglinger, H. Redl, S. Teuschl-Woller, Mater. Sci. Eng.: C **71**, 84–92 (2017). https://doi.org/10.1016/j.msec.2016.09.071
19. J. Wu, X. Liu, Q. Sun, L. Wang, F. Chen, Colloids Surf. B: Biointerfaces **169**, 233–241 (2018). https://doi.org/10.1016/j.colsurfb.2018.05.027
20. H. Yu, X. Zeng, C. Deng, C. Shi, J. Ai, W. Leng, Biomed. Pharmacother. **98**, 325–332 (2018). https://doi.org/10.1016/j.biopha.2017.12.075
21. Y. Deng, X. Song, H. Gan, X. Wang, Y. Xu, Chem. Mater. **32**, 2180–2193 (2020). https://doi.org/10.1021/acs.chemmater.0c00290
22. D.M. Devine, J. Hahn, R.G. Richards, H. Gruner, R. Wieling, S.G. Pearce, J. Biomed. Mater. Res. B **101**, 591–598 (2013). https://doi.org/10.1002/jbm.b.32861
23. C.-M. Han, Y. Xu, J. Tang, X. Ma, X. Liu, Biomaterials **31**, 3465–3470 (2010). https://doi.org/10.1016/j.biomaterials.2009.12.030
24. X. Wei, Y. Zhou, J. Ma, J. Li, M. Wang, Y. Li, Bioact. Mater. **20**, 16–28 (2023). https://doi.org/10.1016/j.bioactmat.2022.05.011
25. N.T. Evans, K.L. Torstrick, D.L. Safranski, T.L. Gall, S.K. Kessler, D.J. Kelly, Acta Biomater. **13**, 159–167 (2015). https://doi.org/10.1016/j.actbio.2014.11.030
26. S. Mo, X. Wang, J. Liu, X. Zhang, Y. Wang, Y. Li, Mater. Horiz. **10**, 881–888 (2023). https://doi.org/10.1039/D2MH01147F
27. A. Rasool, S. Kossar, R. Amiruddin, in *Handbook of Emerging Materials for Semiconductor Industry*. ed. by Y.S. Song, L.R. Thoutam, S. Tayal, S.B. Rahi, T.S.A. Samuel (Springer, Singapore, 2024), pp.165–177. https://doi.org/10.1007/978-981-99-6649-3_14
28. T. Geremew, J3DPA **1**, 1–24 (2022). https://doi.org/10.14302/issn.2831-8846.j3dpa-22-4066
29. M. Qadir, Y. Li, C. Wen, Acta Biomater. **89**, 14–32 (2019). https://doi.org/10.1016/j.actbio.2019.03.006
30. A.A. Harumningtyas, T. Ito, M. Ikuta, T. Kaito, S. Hamaguchi, Plasma Med. **13**, 53–67 (2023). https://doi.org/10.1615/PlasmaMed.2023051355
31. Y. Li, X. Zhang, J. Sun, Y. Zhou, H. Zhang, Acta Biomater. **119**, 432–443 (2021). https://doi.org/10.1016/j.actbio.2020.10.030
32. S.P. Nielsen, Bone **35**, 583–588 (2004). https://doi.org/10.1016/j.bone.2004.04.026
33. I. Pernicova, E.T. Middleton, M. Aye, Osteoporos Int. **19**, 1811–1812 (2008). https://doi.org/10.1007/s00198-008-0734-8
34. J.Y. Reginster, O. Brandi, J. Cannata-Andía, R. Rizzoli, J. Clin. Endocrinol. Metab. **90**, 2816–2822 (2005). https://doi.org/10.1210/jc.2004-1774
35. V. Offermanns, B. Jansen, R.M. Heiß, S. El Khassawna, T.P. Luedemann, Acta Biomater. **69**, 385–394 (2018). https://doi.org/10.1016/j.actbio.2018.01.049
36 Y. Sun, W. Wang, X. Li, C. Wang, Y. Li, Regen. Biomater. **8**, rbaa043 (2021). https://doi.org/10.1093/rb/rbaa043
37. X. Wang, L. Liu, T. Wu, H. Zhu, J. Zhang, Biomed. Mater. **17**, (2022). https://doi.org/10.1088/1748-605X/ac61fb
38. S. Wang, X. Wang, Y. Deng, Z. Zhang, Y. Zhou, Colloids Surf. B: Biointerfaces **176**, 38–46 (2019). https://doi.org/10.1016/j.colsurfb.2018.12.056
39. T. Chen, Y. Zhang, W. Zhang, J. Wu, X. Liu, ACS Biomater. Sci. Eng. **10**, 825–837 (2024). https://doi.org/10.1021/acsbiomaterials.3c01684
40. H. Zhu, J. Sun, W. Liu, H. Wang, Nat. Protoc. **5**, 550–560 (2010). https://doi.org/10.1038/nprot.2009.238
41 A.D. Bakker, J. Klein-Nulend, in *Bone Research Protocols*, vol. 816, ed. by M.H. Helfrich, S.H. Ralston (Humana Press, 2012), pp.19–29. https://doi.org/10.1007/978-1-61779-415-5_2
42. S. Kawasaki, Y. Inagaki, M. Akahane, A. Furukawa, H. Shigematsu, Y. Tanaka, BMC Musculoskelet. Disord. **21**, 692 (2020). https://doi.org/10.1186/s12891-020-03716-1
43. T. Kokubo, H. Takadama, Biomaterials **27**, 2907–2915 (2006). https://doi.org/10.1016/j.biomaterials.2006.01.017
44. Y. Xin, J. Jiang, K. Huo, T. Hu, P.K. Chu, ACS Nano **3**, 3228–3234 (2009). https://doi.org/10.1021/nn9007675
45. J. Anderson, B. Kahn, T. LaBone, L. Brown, F. Harris, Health Phys. **76**, 628–634 (1999). https://doi.org/10.1097/00004032-199906000-00005
46. Y. Li, X. Zhang, J. Sun, Y. Zhou, H. Zhang, Int. J. Nanomedicine **10**, 4549–4563 (2015). https://doi.org/10.2147/IJN.S84398
47. S. Sahoo, A. Sinha, M. Das, J. Mech. Behav. Biomed. Mater. **102**, 103494 (2020). https://doi.org/10.1016/j.jmbbm.2019.103494
48 J. Braux, A. Rofidal, N. Baud'Huin, F. Borel, Acta Biomater. **7**, 2593–2603 (2011). https://doi.org/10.1016/j.actbio.2011.02.013
49. M. Schumacher, A. Lode, A. Helth, M. Gelinsky, Acta Biomater. **9**, 9547–9557 (2013). https://doi.org/10.1016/j.actbio.2013.07.027
50. E. Bonnelye, A. Chabadel, F. Saltel, P. Jurdic, Bone **42**, 129–138 (2008). https://doi.org/10.1016/j.bone.2007.08.043
51. Y. Tsutsumi, D. Nishimura, H. Doi, N. Nomura, T. Hanawa, Mater. Sci. Eng.: C **29**, 1702–1708 (2009). https://doi.org/10.1016/j.msec.2009.01.016
52. T. Hanawa, M. Ota, Biomaterials **12**, 767–774 (1991). https://doi.org/10.1016/0142-9612(91)90028-9
53. X. Cui, Y. Wang, J. Zhang, L. Li, H. Sun, Dent. Mater. **25**, 80–86 (2009). https://doi.org/10.1016/j.dental.2008.04.012
54. T. Hanawa, Sci. Technol. Adv. Mater. **23**, 457–472 (2022). https://doi.org/10.1080/14686996.2022.2106156
55. G. Sundell, C. Dahlin, M. Andersson, M. Thuvander, Acta Biomater. **48**, 445–450 (2017). https://doi.org/10.1016/j.actbio.2016.11.044
56. R. Olivares-Navarrete, L. Hyzy, J. Gittens, Z. Berg, D. Schneider, Biomaterials **31**, 2728–2735 (2010). https://doi.org/10.1016/j.biomaterials.2009.12.029
57. H. Liu, T.J. Webster, Biomaterials **28**, 354–369 (2007). https://doi.org/10.1016/j.biomaterials.2006.08.049